

## Three-dimensional scattering-assisted tunneling in resonant-tunneling diodes

Patrick Roblin and Wan-Rone Liou

*Department of Electrical Engineering, The Ohio State University, Columbus, Ohio 43210*

(Received 6 December 1991; revised manuscript received 14 August 1992)

A quantum model and simulator for resonant tunneling diodes that includes three-dimensional (3D) scattering-assisted tunneling processes is reported. The 3D phase-breaking or quasi-phase-breaking scattering processes considered are polar scattering by optical phonons, deformation potential scattering by acoustic phonons, interface roughness scattering, and alloy scattering. The simulator solves Schrödinger equation in 3D using an expansion in terms of sequential scattering events. The average transmission and reflected currents are then calculated using an (analytic) ensemble average over the scatterers. We assume that the scattering events are uncorrelated and use a semiclassical phonon field. The relaxation approximation is not used. Back scattering is included so that the current is conserved. An important feature is that the 3D analysis permits one to account for the variation of the perpendicular momentum of the electron in the scattering process. This variation of the perpendicular momentum and the dependence of the scattering process upon the initial perpendicular momentum are the source of the broadening of the transmission coefficient. Simulation results are reported for a 34/34/34 and a 50/50/50 double-barrier heterostructure. The dominant scattering mechanisms in these devices are polar phonon scattering and interface roughness scattering. Polar phonon-assisted tunneling is revealed in the transmission coefficient by the presence of secondary resonant transmission peaks due to emission and absorption of optical phonons. At low temperature (4.2 K) this emission-assisted tunneling introduces a noticeable bump in the current voltage characteristics of the diode in agreement with a previous one-dimensional quantum model and low-temperature experimental data. At room temperature, however, 3D polar scattering introduces a much larger broadening of the transmission peak in the 50/50/50 structure than can be predicted by a one-dimensional model. A strong broadening is also introduced by interface scattering for monolayer terraces of 70 Å average width, emphasizing the importance of the interface quality. Up to 6 and 20 multiple sequential IR scattering events are required for the transmission coefficient to fully converge for the 34- and 50-Å barrier diodes resulting in a transmission coefficient versus energy with a characteristic asymmetric shape. However, the diode IV current converges typically in only three sequential IR scattering events. As expected the effective broadening introduced by these scattering mechanisms reduces the peak current and increases the valley current of the current voltage characteristic of the resonant tunneling diodes in agreement with experimental data.

### I. INTRODUCTION

Heterostructure devices of small size have been instrumental in revealing the wave nature of electrons as predicted by quantum mechanics. The resonant tunneling diode demonstrated by Chang, Esaki, and Tsu<sup>1</sup> and the Bloch oscillator proposed by Esaki and Tsu<sup>2</sup> are examples of novel semiconductor devices which rely on the wave nature of the electron. Other electron devices, such as the Zener oscillator,<sup>3</sup> are also conceptually possible.

Modern growth techniques now permit the fabrication of high quality one-dimensional heterostructures. They have led to improvement of the resonant tunneling diode by Sollner *et al.*<sup>4</sup> and more recently the demonstration of the Bloch oscillator by Sibille, Palmier, and Wang<sup>5</sup> and Beltram *et al.*<sup>6</sup> at room temperature. Limitations on the operation of these devices remain due to the scattering processes. An improved understanding of scattering processes is therefore critical for the design of optimal devices structures.

In this paper we present a three-dimensional (3D) quantum simulator which permits us to analyze the impact of the scattering processes upon tunneling in a het-

erostructure. In this study we will consider polar scattering by longitudinal optical phonons, deformation potential scattering by longitudinal acoustic phonons, interface roughness scattering, and alloy scattering. A similar study recently reported by Chevoir and Vinter,<sup>7</sup> also includes the 3D effect but it is based on approximate scalar rate equations (semiclassical model), whereas our quantum simulator directly solves the Schrödinger equation and therefore includes backscattering (self-energy effects and current conservation).

Many other approaches have been used to solve the Schrödinger equation in the presence of scattering, but with concomitant limitations. Frensley<sup>8</sup> and Jensen and Buot<sup>9</sup> used the Wigner distribution formalism. It leads to strongly nonlinear equations in the presence of dissipative effects, however, and the Wigner distribution has only been solved so far using the relaxation time approximation and assuming a constant relaxation time. Other approaches based on the Green-function formalism only admit solution for simplified device or scattering models. For example Wingreen, Jacobsen, and Wilkins<sup>10</sup> (polar scattering) and Leo and MacDonald<sup>11</sup> (interface roughness scattering) both use a simplified hopping model for

the resonant tunneling diode. Datta<sup>12</sup> assumes that the electron-phonon interaction can be approximated by an impulse function in space. Another limitation is that these analyses<sup>8-10,12</sup> are one dimensional. As we shall see, three-dimensional effects must be accounted for if one is to simulate the broadening of the transmission coefficient introduced by scattering processes in some modes of operation.

Consider the case of polar scattering. A multiphonon studies accounting for phonon-assisted tunneling was reported by Wingreen, Jacobsen, and Wilkins for electron tunneling through a double barrier. Such a model is consistent with the experimental results obtained at low temperature (4.2 K) by Goldman, Tsui, and Cunningham.<sup>13</sup> Alternately at room temperature and at 77 K, device physicists (see the discussions given by Stone and Lee,<sup>14</sup> Vinter and Weil,<sup>15</sup> and Mizuta, Tanoue, and Takahashi<sup>16</sup>) have found the need to introduce an effective broadening in the transmission peak to improve the fit between the measured and calculated current-voltage characteristics of multibarrier resonant tunneling diodes. The main consequence of this energy broadening is to reduce the peak to valley ratio of the current-voltage characteristics of the resonant tunneling diodes.

The one-dimensional model of Wingreen, Jacobsen, and Wilkins<sup>10</sup> cannot account for this broadening at room temperature. In this paper we shall demonstrate that a three-dimensional model of phonon scattering permits us to reproduce both the low- and high-temperature results. The multiphonon model reported by Ref. 10 relies on a one-dimensional (in space) model for the electron which assumes that the perpendicular momentum of the electron is left unchanged:  $\mathbf{k}_{1\perp} = \mathbf{k}_{0\perp}$  (0, incident; 1, scattered). It results that the longitudinal part of the energy  $E_1$  could only assume two values  $E_{1x} = E_{0x} \pm \hbar\omega_q$  for a single-phonon scattering event. We shall see that in one-dimensional heterostructures the perpendicular momentum satisfies instead the two-dimensional momentum conservation rule:  $\mathbf{k}_{1\perp} = \mathbf{k}_{0\perp} \pm \mathbf{q}_\perp$ . The various new scattered states which result when the perpendicular momentum is allowed to vary can greatly affect the tunneling process. Indeed the longitudinal electron energy  $E_{1x}$  can then take continuous values within a prescribed range,

$$E_{1x} \leq E_{0x} \pm \hbar\omega_q + \frac{\hbar^2 k_{0\perp}^2}{2m^*}. \quad (1)$$

As we shall see, the three-dimensional effects discussed above for phonon scattering apply also to elastic scattering processes.

In this paper we study 3D scattering-assisted tunneling in a simple double-barrier heterostructure. In Sec. II we present the heterostructure. In Sec. III we develop the 3D scattering-assisted tunneling theory. In Sec. IV we discuss the various scattering processes under consideration. An effective transmission coefficient for 3D scattering-assisted tunneling is introduced in Sec. V. The numerical algorithm is described in Sec. VI. Simulation results are presented in Sec. VIII for two double-barrier diodes. We conclude in Sec. IX by summarizing the results obtained.

## II. TEST RESONANT-TUNNELING STRUCTURE

To test the scattering-assisted tunneling simulator proposed below we will employ a resonant-tunneling diode (see Fig. 1) consisting of a conventional undoped AlGaAs/GaAs/AlGaAs double-barrier structure sandwiched between two strongly doped GaAs  $n^+$  buffers.

We consider two double-barrier structures with a barrier width and a well width of six and nine lattice parameters wide ( $\approx 34$  and  $50$  Å), respectively. A barrier height of 0.25 eV corresponding to an Al mole fraction of 0.3 is used. The simple tight-binding band [see Eq. (6)] with the effective mass of  $0.076 + 0.1m$  the electron rest mass is used for  $\text{Al}_m\text{Ga}_{1-m}\text{As}$ .

As shown in Fig. 1 the voltage  $V_D$  applied across the resonant tunneling diode Fermi levels  $E_{fL}$  and  $E_{fR}$  is given by

$$V_D = V_{DI} + E_{fcL} - E_{fcR}, \quad (2)$$

where  $V_{DI}$  is the intrinsic voltage appearing across the double-barrier structure and with  $E_{fcL}$  and  $E_{fcR}$  the built-in potentials in the buffers. A donor concentration  $N_D = 10^{18} \text{ cm}^{-3}$  is used in the buffers. For this high concentration the donor ionization energy vanishes, and the donors can be assumed to be completely ionized.<sup>15</sup>

We assume that the electric field is constant inside the quantum structure. Note that there is no undoped spacer between the double barrier and the buffers in the test device. A self-consistent calculation of the potential and field across the device becomes necessary in the presence of these spacers.

## III. SCATTERING-ASSISTED TUNNELING THEORY

### A. Heterostructure model

We wish to study the scattering-assisted tunneling process in a heterostructure. The total semiclassical Hamiltonian of one electron submitted to scattering by various elastic and inelastic scattering processes  $i$  is the sum of the electron Hamiltonian  $H_e$  and the electron-scattering interaction Hamiltonian

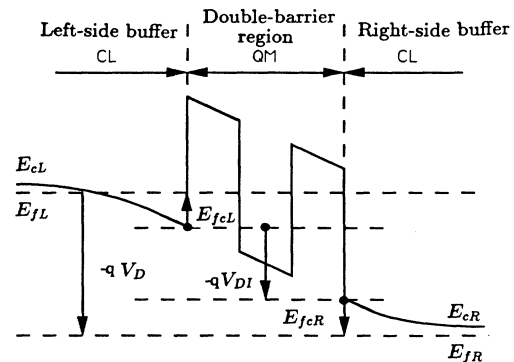


FIG. 1. Band diagram of the test resonant-tunneling structure.

$$H = H_e + \sum_i H_{e-ph,i}(t) + \sum_i H_{elast,i}.$$

The time dependence of the electron-phonon scattering process interaction term  $H_{e-ph,i}(t)$  will result from our assumption of a classical field of lattice vibrations which remains in thermal equilibrium despite its interaction with the electrons. We must now solve the time-dependent Schrödinger equation

$$H|\Psi\rangle = i\hbar \frac{d}{dt}|\Psi\rangle \quad (3)$$

in the superlattice region. Here the heterostructure is spatially varying along the superlattice axis  $x$  and is uniform in the perpendicular direction ( $y$  and  $z$ ). To analyze such one-dimensional superlattices it is convenient to use the generalized Wannier picture.<sup>18</sup> In this picture the electron wave function  $|\Psi\rangle$  is expanded in terms of the generalized Wannier functions  $|\mathbf{k}_\perp, n\rangle$  using the envelope function  $f(\mathbf{k}_\perp, n, t)$ ,

$$|\Psi\rangle = \sum_n \int f(\mathbf{k}_\perp, n, t) |\mathbf{k}_\perp, n\rangle d\mathbf{k}_\perp. \quad (4)$$

Here we are limiting this expansion to a single generalized band. In a uniform crystal the state  $|\mathbf{k}_\perp, n\rangle$  is a generalized Wannier function at the lattice site  $n$  along the superlattice direction and a Bloch state  $\mathbf{k}_\perp$  in the perpendicular direction.<sup>18</sup> Like the Wannier functions these generalized Wannier functions are orthogonal

$$\langle \mathbf{k}'_\perp, n' | \mathbf{k}_\perp, n \rangle = \delta_{n'n} \delta(\mathbf{k}'_\perp - \mathbf{k}_\perp)$$

and are assumed here to form a complete basis (generalized one-band approximation). In this work we postulate the existence of these states. The existence of the generalized Wannier functions in heterostructures has been rigorously demonstrated in the case of one-dimensional crystals.<sup>19,20</sup> In three-dimensional crystals with a potential varying in one dimension the generalized Wannier functions can still be labeled with the perpendicular wave vector  $\mathbf{k}_\perp$  because the crystal Hamiltonian is translation invariant in the transverse direction and therefore commutes with the transverse translation operator.

As for Wannier functions, the matrix element of the heterostructure Hamiltonian  $H_e$  in the generalized Wannier function basis is

$$\langle \mathbf{k}'_\perp, n' | H_e | \mathbf{k}_\perp, n \rangle = H_{n'n}^e(\mathbf{k}_\perp) \delta(\mathbf{k}'_\perp - \mathbf{k}_\perp)$$

with [assuming slowly varying  $V(x)$ ]

$$H_{n'n}^e(\mathbf{k}_\perp) = H_{n'n}^0(\mathbf{k}_\perp) - eV(na) \delta_{n'n},$$

where  $H_{n'n}^0(\mathbf{k}_\perp)$  is the matrix element of the unbiased heterostructure (generalized band structure) and where  $V(x)$  is the applied electrostatic potential sampled at the lattice site  $x=na$ . In a homojunction superlattice the band structure does not vary with position and the matrix element  $H_{n'n}^0(\mathbf{k}_\perp)$  is simply given by

$$H_{n'n}^0(\mathbf{k}_\perp) = \mathcal{E}_{n-n}(\mathbf{k}_\perp),$$

where  $\mathcal{E}_m(\mathbf{k}_\perp)$  are the Fourier coefficients of the band structure  $\mathcal{E}(\mathbf{k})$ ,

$$\mathcal{E}(\mathbf{k}) = \sum_{m=-N_B}^{N_B} \mathcal{E}_m(\mathbf{k}_\perp) e^{ik_x ma} \quad (5)$$

with  $N_B$  the number of Fourier coefficients to which the band structure  $\mathcal{E}(\mathbf{k})$  is truncated.

In a general superlattice device the generalized band structure varies with position. For simplicity of presentation we shall now assume that the generalized band structure is well represented by an effective mass approximation in the transverse direction so that we have

$$H_{n'n}^e(\mathbf{k}_\perp) = H_{n'n} + \left[ \frac{\hbar^2 k_\perp^2}{2m^*(n)} \right] \delta_{n'n}.$$

In the demonstration example selected later in this paper we use the tight binding band structure  $\mathcal{E}(k_x) = A(n) + E_c(na) - A(n) \cos k_x a$  where  $E_c(na)$  is the conduction band edge potential  $E_c(x)$  sampled at the lattice site  $x=na$  and where  $A(n)$  is the amplitude of the band at the site  $n$  is given from the effective mass  $m^*(n)$  according to  $A(n) = \hbar^2 / [m^*(n)a^2]$ . The mass is spatially varying and a Hermitian Hamiltonian is obtained using the effective mass matching theory developed by Kroemer.<sup>21</sup>  $H_{n'n}$  is

$$\begin{aligned} H_{n'n} = & -\frac{\hbar^2}{2a^2 \sqrt{m^*(n)m^*(n+1)}} \delta_{n'n+1} \\ & -\frac{\hbar^2}{2a^2 \sqrt{m^*(n)m^*(n-1)}} \delta_{n'n-1} \\ & + \left[ \frac{\hbar^2}{a^2 m^*(n)} + E_c(na) - eV(na) \right] \delta_{n'n}. \end{aligned} \quad (6)$$

See Ref. 22 for more complex (complete) band structures ( $N_B > 1$ ).

In order to handle the longitudinal variation of the transversal mass it is convenient to treat the effective spatial variation of the transversal kinetic energy like an effective longitudinal potential

$$H_{n'n}^e(\mathbf{k}_\perp) = \tilde{H}_{n'n} + \left[ \frac{\hbar^2 k_\perp^2}{2m^*(0)} \right] \delta_{n'n},$$

where  $\tilde{H}_{n'n}$  is defined using

$$\tilde{H}_{n'n} = H_{n'n} + \frac{\hbar^2 k_\perp^2}{2m^*(0)} \left[ \frac{m^*(0)}{m(n)} - 1 \right] \delta_{n'n}.$$

## B. Ensemble average scattering model

Let us consider inelastic scattering by phonons and elastic scattering by structural defects. As we shall see below, both scattering processes can be analyzed in a similar fashion.

We assume that the electron is coupled to classical lattice vibrations. However, we use the coupling coefficients derived when the electron is coupled to quantized lattice vibrations or phonons. This semiclassical treatment neglects the quantum noise associated with the random thermal distribution of the lattice vibration over the various phonon states  $|N_q\rangle$  for a given mode  $q$ . The

electron-phonon interaction Hamiltonian is

$$H_{e-ph} = \frac{i}{\sqrt{\Omega}} \sum_{\mathbf{q}} \alpha_{\mathbf{q}} \{ a_{\mathbf{q}} e^{i\mathbf{q} \cdot \mathbf{r}} - a_{\mathbf{q}}^{\dagger} e^{-i\mathbf{q} \cdot \mathbf{r}} \}, \quad (7)$$

where  $a_{\mathbf{q}}$  and  $a_{\mathbf{q}}^{\dagger}$  are, respectively, the destruction and creation operators for the phonon of mode  $\mathbf{q}$ ,  $\mathbf{r}$  is the electron position operator,  $\Omega$  the lattice volume,  $\alpha_{\mathbf{q}}$  is the interaction weight for the phonon wave vector  $\mathbf{q}$  (see Sec. III). Only bulk phonons are considered here. Scattering by localized and interface phonon modes is also expected to contribute<sup>24,25</sup> but the coupling constants (e.g., Fröhlich constant for polar scattering) have not yet been evaluated.

The semiclassical picture for the phonon interaction Hamiltonian is obtained by performing the following substitution:

$$\begin{aligned} a_{\mathbf{q}} &= A_{\mathbf{q}\pm} e^{-i(\omega_{\mathbf{q}}t + \phi_{\mathbf{q}})}, \\ a_{\mathbf{q}}^{\dagger} &= A_{\mathbf{q}\pm} e^{i(\omega_{\mathbf{q}}t + \phi_{\mathbf{q}})}, \end{aligned}$$

where  $A_{\mathbf{q}\pm}$  is the lattice vibration amplitude of mode  $\mathbf{q}$  with frequency  $\omega_{\mathbf{q}}$  and phase  $\phi_{\mathbf{q}}$ . Note that in this substitution we consider two possible amplitudes  $A_{\mathbf{q}+}$  and  $A_{\mathbf{q}-}$  because we intend to use the quantum result that the phonon emission and absorption rates are weighted by the factor  $1 + N_{\text{ph}}$  and  $N_{\text{ph}}$ , respectively.  $A_{\mathbf{q}+}$  will be used for both  $a_{\mathbf{q}}$  (scattering) and  $a_{\mathbf{q}}^{\dagger}$  (backscattering) when these operators contribute to the absorption of a phonon by the incident electron.  $A_{\mathbf{q}-}$  will be used for both  $a_{\mathbf{q}}^{\dagger}$  (scattering) and  $a_{\mathbf{q}}$  (backscattering) when these operators contribute to the emission of a phonon by the incident electron.

After substitution the following semiclassical interaction Hamiltonian is obtained:

$$H_{e-ph} = \frac{2}{\sqrt{\Omega}} \sum_{\mathbf{q}} \alpha_{\mathbf{q}} A_{\mathbf{q}\pm} \sin(\omega_{\mathbf{q}}t - \mathbf{q} \cdot \mathbf{r} + \phi_{\mathbf{q}}). \quad (8)$$

Note that the amplitude  $A_{\mathbf{q}\pm}$  and the phase  $\phi_{\mathbf{q}}$  are randomly updated at times set by the phonon lifetimes. For optical phonons we have  $\Delta\omega = 0.012\omega_{\text{LO}}$ .<sup>17</sup> The corresponding phonon lifetime is 8.3 ps and the resulting energy broadening is on the order of 0.5 meV. For a given device this introduces a noise in the dc current. Since we are only interested here in the average current, a simpler model is obtained by assuming that the phonons' amplitude  $A_{\mathbf{q}\pm}$  and phonons' phase  $\phi_{\mathbf{q}}$  are randomly distributed and mutually uncorrelated. The average current is then obtained from an ensemble average over the phonons' amplitude and phase using

$$\langle \mathbf{k}'_1, n' | H_{e-ph} | \mathbf{k}_1, n \rangle = \frac{1}{\sqrt{\Omega}} \sum_{q_x > 0} \sin(q_x n' a) \delta_{n'n} \sum_{\mathbf{q}_1} C_{\pm}(\mathbf{q}) \{ \delta(\mathbf{k}'_1 - \mathbf{k}_1 + \mathbf{q}_1) e^{i(\omega_{\mathbf{q}}t + \phi_{\mathbf{q}})} + \delta(\mathbf{k}'_1 - \mathbf{k}_1 - \mathbf{q}_1) e^{-i(\omega_{\mathbf{q}}t + \phi_{\mathbf{q}})} \}.$$

A similar model is developed for elastic scattering. A general elastic scattering process can be represented by an interaction potential  $H_{\text{elast}}(\mathbf{r})$ . It is convenient to use periodic boundary conditions so that we have

$$H_{\text{elast}} = \sum_{\mathbf{q}} V_{\mathbf{q}} e^{i\mathbf{q} \cdot \mathbf{r}} = \sum_{\mathbf{q}} |V_{\mathbf{q}}| e^{i\phi_{\mathbf{q}}} e^{i\mathbf{q} \cdot \mathbf{r}},$$

$$\begin{aligned} \langle A_{\mathbf{q}'\pm} e^{i\phi_{\mathbf{q}'}} A_{\mathbf{q}\pm} e^{-i\phi_{\mathbf{q}}} \rangle_{\text{EA}} &= \langle A_{\mathbf{q}\pm}^2 \rangle_{\text{EA}} \delta_{\mathbf{q}'\mathbf{q}} \\ &= (N_{\mathbf{q}} + \frac{1}{2} \mp \frac{1}{2}) \delta_{\mathbf{q}'\mathbf{q}}, \end{aligned} \quad (9)$$

$$\langle A_{\mathbf{q}'\pm} e^{i\phi_{\mathbf{q}'}} A_{\mathbf{q}\pm} e^{i\phi_{\mathbf{q}}} \rangle_{\text{EA}} = 0,$$

where  $N_{\mathbf{q}}$  is the average number of phonons in the mode  $\mathbf{q}$ . The notation  $\langle \rangle_{\text{EA}}$  indicates the ensemble average over the scattering events.

The number of phonons of frequency  $\omega_{\mathbf{q}}$  is given by the Bose-Einstein thermal distribution

$$N_{\mathbf{q}} = \frac{1}{\exp\left[\frac{\hbar\omega_{\mathbf{q}}}{k_B T_0}\right] - 1}$$

with  $k_B$  the Boltzmann constant and  $T_0$  the lattice temperature.

The phonon field extends over the entire heterostructure system (sample) of length  $L_x$ . Note, however, that we shall only study the interaction between electrons and phonons in the superlattice region (e.g., double barrier) whose length  $L_{\text{SL}}$  is generally much smaller than  $L_x$ . It is convenient to assume that the lattice vibrations vanish at the edges of the sample. Using  $\phi_{q_x, q_1} = \phi_{-q_x, q_1} + \pi$  we obtain the desired standing waves

$$H_{e-ph} = \frac{2}{\sqrt{\Omega}} \sum_{q_x > 0} \sum_{\mathbf{q}_1} C_{\pm}(\mathbf{q}) \cos(\omega t - \mathbf{q}_1 \cdot \mathbf{r}_1 + \phi_{\mathbf{q}}) \sin(q_x x),$$

where we have introduced the constant

$$C_{\pm}(\mathbf{q}) = 2\alpha_{\mathbf{q}} A_{\mathbf{q}\pm}. \quad (10)$$

$q_x$  is now quantized  $q_x L = q_x N a = p\pi$  and given by

$$q_x = \frac{p\pi}{L} = \frac{p}{N} \frac{\pi}{a} \quad \text{for } 0 \leq p \leq \frac{N}{2}. \quad (11)$$

The number of  $q_x$  modes in the sample is given by half the number of lattice sites. If the sample length  $L_x$  is large enough compared to  $L_{\text{SL}}$ , the phonon momentum quantization does not affect the phonon-assisted tunneling process. The length of the sample  $L_x$  then becomes arbitrary. Indeed, the increase in the number of modes  $q_x$  resulting from an increase of  $L_x$  is compensated in  $H_{\text{int}}$  by the decrease in the polar interaction strength since we have  $\Omega = L_x S$  where  $S = L_y L_z$  is the superlattice area and  $L_x$  its length.

In the generalized Wannier function basis the matrix element of the electron-phonon interaction is (the phonon scattering index  $i$  is dropped for simplicity)

where  $\mathbf{q}$  is a reciprocal space vector. The phase  $\phi_{\mathbf{q}}$  and the amplitude of  $|V_{\mathbf{q}}|$  will vary from device to device due to the random spatial distribution of the scattering agents (e.g., alloy scattering and interface roughness scattering). An ensemble average over the scatterers is then used to calculate the average transmission and reflected currents.

The analysis of elastic scattering thus becomes similar to that of a phase-breaking scattering process.

In the generalized Wannier function basis the matrix element of the elastic phase scattering process  $i$  at lattice  $N_i$  is

$$\langle \mathbf{k}'_l, n' | H_{\text{elast}, i} | \mathbf{k}_l, n \rangle = \delta_{n'N_i} \delta_{n'n} \frac{1}{\sqrt{S}} \sum_{\mathbf{q}_l} C_i(\mathbf{q}_l) \delta(\mathbf{k}'_l - \mathbf{k}_l - \mathbf{q}_l),$$

where Hermiticity requires  $C_i(-\mathbf{q}_l) = C_i^*(\mathbf{q}_l)$ . In this work we assume that the elastic scattering events are uncorrelated,

$$\langle C_i(\mathbf{q}'_l) C_i(\mathbf{q}_l) \rangle_{\text{EA}} = \langle |C_i(\mathbf{q}_l)|^2 \rangle_{\text{EA}} \delta_{-\mathbf{q}'_l \mathbf{q}_l} \delta_{i'i}. \quad (12)$$

Specific expressions for interface roughness scattering and alloy scattering are given in Sec. III.

### C. The envelope equations

Now that the Hamiltonian matrix elements have been calculated we can rewrite the Schrödinger equation (3) in the generalized Wannier function basis (4). This gives for the envelope function  $f(\mathbf{k}_l, n, t)$ , the following envelope equation:

$$\begin{aligned} i\hbar \frac{d}{dt} f(\mathbf{k}_l, n, t) = & \frac{\hbar^2 \mathbf{k}_l^2}{2m^*(0)} f(\mathbf{k}_l, n, t) + \sum_{n'=-N_B}^{N_B} \tilde{H}_{nn'} f(\mathbf{k}_l, n', t) \\ & + \frac{1}{\sqrt{\Omega}} \sum_{q_x > 0} \sin(q_x n a) \sum_{\mathbf{q}_l} C_{\pm}(\mathbf{q}) \{ f(\mathbf{k}_l + \mathbf{q}_l, n, t) e^{i(\omega_q t + \phi_q)} + f(\mathbf{k}_l - \mathbf{q}_l, n, t) e^{-i(\omega_q t + \phi_q)} \} \\ & + \frac{1}{\sqrt{S}} \sum_i \delta_{nN_i} \sum_{\mathbf{q}_l} C_i(\mathbf{q}_l) f(\mathbf{k}_l - \mathbf{q}_l, n, t). \end{aligned} \quad (13)$$

As usual the magnitude of the envelope function  $|f(\mathbf{k}_l, n, t)|^2$  gives the probability of presence at the lattice site  $n$ , and at time  $t$  of an electron with a perpendicular momentum  $\mathbf{k}_l$ .

This envelope equation is the generalized Schrödinger equation which we must solve to analyze scattering-assisted tunneling in a superlattice. We know that the electron absorbs or emits optical phonons so that its energy will be either increased or decreased by a multiple of  $\hbar\omega_q$  when it is scattered by a phonon. For elastic scattering the total energy remains unchanged. Therefore a steady-state solution can be obtained by expanding the envelope function into a Fourier series. We shall initially limit our analysis to a single sequential scattering event (the generalization to multiple sequential events is considered afterward). Consider the envelope function given below

$$\begin{aligned} f(n, \mathbf{k}_l, t) = & f_0(n) \delta(\mathbf{k}_l - \mathbf{k}_{l0}) e^{-i(E_0 t / \hbar)} \\ & + \frac{1}{\sqrt{\Omega}} e^{-i(E_0 t / \hbar)} \sum_{q_x > 0} \sum_{\mathbf{q}_l} e^{-i(\omega_q t + \phi_q)} C_+(\mathbf{q}) f_1(n, \mathbf{q}_l, q_x) \delta(\mathbf{k}_l - (\mathbf{k}_{l0} + \mathbf{q}_l)) \\ & + \frac{1}{\sqrt{\Omega}} e^{-i(E_0 t / \hbar)} \sum_{q_x > 0} \sum_{\mathbf{q}_l} e^{i(\omega_q t + \phi_q)} C_-(\mathbf{q}) f_1(n, \mathbf{q}_l, q_x) \delta(\mathbf{k}_l - (\mathbf{k}_{l0} - \mathbf{q}_l)) \\ & + \frac{1}{\sqrt{S}} e^{-i(E_0 t / \hbar)} \sum_i \sum_{\mathbf{q}_l} C_i(\mathbf{q}_l) f_1(n, \mathbf{q}_l, i) \delta(\mathbf{k}_l - (\mathbf{k}_{l0} + \mathbf{q}_l)). \end{aligned} \quad (14)$$

We can easily demonstrate that  $f(\mathbf{k}_l, n, t)$  is an ensemble average solution of the envelope equation (13) limited to a single sequential scattering event provided that  $f_0$  and  $f_1$  are solutions of specific envelope equations. To obtain these envelope equations we first substitute the proposed solution (14) in the envelope equation (13), and equate the terms of same energy (frequency)  $E_0$ ,  $E_0 + \hbar\omega_q$ , and  $E_0 - \hbar\omega_q$ , and weighted by the same Dirac function  $\delta(\mathbf{k}_l - \mathbf{k}'_l)$  (i.e., same perpendicular Bloch wave). Next we perform an ensemble average using Eqs. (9) and (12) assuming that elastic and phonon scattering are uncorrelated processes

$$\langle C_i(\mathbf{q}'_l) C_{\pm, \mp}(\mathbf{q}) e^{\pm i\phi_{q'}} \rangle_{\text{EA}} = 0.$$

It results that  $f_0$  must satisfy the envelope equation

$$\begin{aligned} E_{0x} f_0(n) = & \sum_{n'} \tilde{H}_{nn'} f_0(n') \\ & + \frac{1}{L_x} \sum_{q_x > 0} \{ G_+(n, q_x) + G_-(n, q_x) \} \\ & + \sum_i G_i(n), \end{aligned} \quad (15)$$

where  $G_{\pm}$  and  $G_i$  are coupling terms defined below.

The envelope function  $f_1$  is a solution of the envelope equation

$$\begin{aligned} E_{1x} f_1(n, E_{1x}, q_x) = & \sum_{n'} \tilde{H}_{nn'} f_1(n', E_{1x}, q_x) \\ & + \sin(q_x n a) f_0(n) \end{aligned} \quad (16)$$

for phonon scattering and

$$E_{1x}f_1(n, E_{1x}, i) = \sum_{n'} \tilde{H}_{nn'} f_1(n', E_{1x}, i) + \delta_{n, N_i} f_0(n) \quad (17)$$

for elastic scattering.

We have used in Eqs. (15), (16), and (17) the longitudinal incident and scattered energies  $E_{0x}$  and  $E_{1x}$  which are defined to be

$$E_{0x} = E_0 - \frac{\hbar^2}{2m^*(0)} |\mathbf{k}_{0\perp}|^2,$$

$$E_{1x}(\pm \mathbf{q}_\perp) = E_0 \pm \hbar\omega_q - \frac{\hbar^2}{2m^*(0)} |\mathbf{k}_{0\perp} \pm \mathbf{q}_\perp|^2$$

for phonon scattering ,

$$E_{1x}(\mathbf{q}_\perp) = E_0 - \frac{\hbar^2}{2m^*(0)} |\mathbf{k}_{0\perp} + \mathbf{q}_\perp|^2 \text{ for elastic scattering .}$$

In Eq. (15) we have defined the coupling terms  $G_\pm$  and  $G_i$  which are given by

$$G_\pm(n, q_x) = \sin(q_x na) \frac{1}{S} \sum_{\mathbf{q}_\perp} \langle C_\pm^2(\mathbf{q}) \rangle_{\text{EA}} f_1(n, \pm \mathbf{q}_\perp, q_x), \quad (18)$$

$$G_i(n) = \delta_{nN_i} \frac{1}{S} \sum_{\mathbf{q}_\perp} \langle |C_i(\mathbf{q}_\perp)|^2 \rangle_{\text{EA}} f_1(n, \pm \mathbf{q}_\perp, i). \quad (19)$$

The summation over the perpendicular momentum can be replaced by an integration. For all the scattering processes discussed below (except acoustic scattering), the integration over the perpendicular momentum can be carried analytically. The coupling terms are then expressed as

$$G_\pm(n, q_x) = \sin(q_x na) \int_{-2A_L}^{E_0 \pm \hbar\omega_{\text{LO}}} f_1(n, E_{1x}, q_x) \times H_\pm(E_{1x}, q_x) dE_{1x}$$

for optical phonon scattering and

$$G_i(n) = \delta_{nN_i} \int_{-2A_L}^{E_0} f_1(n, E_{1x}, i) H_i(E_{1x}) dE_{1x}$$

$$H_{\text{LO}, \pm}(E_{1x}, q_x) = \frac{m^*}{2\pi\hbar^2} \frac{4\alpha_{\text{LO}}^2(N_q + \frac{1}{2} \mp \frac{1}{2})}{\left[ \left( q_x^2 + \frac{2m}{\hbar^2} (E_{0x} \pm \hbar\omega_{\text{LO}} - E_{1x}) \right)^2 + 4q_x^2 k_{0\perp}^2 \right]^{1/2}}. \quad (21)$$

Electrons in a crystal are also scattered by the displacement of the atoms from their lattice site. The displacement of the atoms induces a local change of the band gap which acts as a potential, scattering the electrons. For longitudinal acoustic phonons (AC) the coupling constant is<sup>26</sup>

$$\alpha_{q, \text{AC}} = \left[ \frac{\hbar\Xi^2}{2\rho\omega_q} \right]^{1/2},$$

where  $\Xi$  is the so-called deformation potential and  $\rho$  the semiconductor density. For GaAs  $\Xi$  is 7 eV (Ref. 27) and

for elastic scattering, where  $H$  is a coupling function specific to the scattering mechanism considered.

Because we have done a full three-dimensional analysis the coupling function  $H$  is found to be a continuous function of  $E_{1x}$  instead of the impulse function obtained in one-dimensional analyses. In practice we replace the lower integration bound  $-2A_L$  by a more physical value (e.g.,  $-0.3$  eV) so as to limit the range of the transversal energy to a physical value.

Note that a complete multiple sequential scattering solution can be obtained using the same procedure. For example a second sequential scattering event is implemented by introducing the coupling terms in the Wannier equations (16) and (17) which couple the waves  $f_1$  to the waves  $f_2$ . The presence of the coupling terms in both the incident as well as the scattered Wannier equations accounts for backscattering. The latter enforces the conservation of the current. This is demonstrated in the Appendix for a single sequential scattering event but holds also for multiple sequential scattering events.

#### IV. SCATTERING PROCESSES CONSIDERED

The first of four scattering processes considered is polar scattering, a mechanism by which an electron is scattered by the longitudinal optical phonons (LO) through the interaction of its Coulomb field with the polarization waves of the lattice. The coupling constant in Eq. (7) is<sup>23</sup> (see Ref. 26 for a review)

$$\alpha_{q, \text{LO}} = e \left\{ \frac{\hbar\omega_{\text{LO}}}{2} \left[ \frac{1}{\epsilon_{\text{opt}}} - \frac{1}{\epsilon_{\text{stat}}} \right] \right\}^{1/2} \frac{1}{q} = \frac{\alpha_{\text{LO}}}{q}, \quad (20)$$

where  $e$  is the electron charge, and  $q$  the amplitude of the phonon wave vector  $\mathbf{q}$ . For GaAs we use for dielectric constants  $\epsilon_{\text{stat}}/\epsilon_{\text{opt}} = 1.1664$ ,<sup>26</sup> and for the optical phonon frequency  $\omega_{\text{LO}}$  assumed independent of  $\mathbf{q}$  (Einstein model), 8.55 THz. The coupling function  $H$  obtained after integration of  $\langle C_{\text{LO}}^2 \rangle_{\text{EA}}$  [see Eqs. (10) and (18)] over the perpendicular momentum is

$\rho$  is 5.37 g/cm<sup>3</sup>.

The number of phonons  $N_q$  given by the Bose-Einstein distribution is determined using the so-called equipartition approximation by

$$N_q \simeq \frac{k_B T_0}{\hbar\omega_q} \text{ for } N_q \gg 1.$$

For long wavelengths ( $q$  small) we have  $\omega_q = qv_s$  with  $v_s$  the sound velocity. Despite the simplicity of the model used, the wave-vector dependent frequency  $\omega_q$  prevents

the integration over the perpendicular momentum to be carried out analytically (see Conwell<sup>28</sup>). We elected to treat acoustic scattering as an elastic scattering process. This overestimates the emission process and underestimates the absorption process. The coupling constant  $H$  obtained after integration of  $\langle C_{AC}^2 \rangle_{EA}$  [see Eqs. (10) and (18)] over the perpendicular momentum is simply

$$H_{AC,\pm}(E_{1x}) \simeq \frac{1}{2\pi} \frac{m^*}{\hbar^2} \left[ \frac{2\Xi^2 k_B T_0}{\rho v_s^2} \right]^{1/2}. \quad (22)$$

Another important scattering process is the scattering of electrons by the roughness of the interface (IR) of two different semiconductors. A distribution of terraces typically of a monolayer thickness is present at the interface.<sup>29</sup> The electron is scattered elastically by these terraces, i.e., the total energy of the electron is conserved. However, the longitudinal and perpendicular energy of the electron changes in the process. Following Leo and MacDonald,<sup>11</sup> consider an interface with a density of terraces  $D_T$  (number of terraces per unit area). Let us assume that the distribution of the terrace's width can be approximated by a Gaussian function of mean  $\sigma$ . If the terraces are mutually uncorrelated (in position and width) the coupling constant is found to be

$$\langle |C_{IR,i}(\mathbf{q}_\perp)|^2 \rangle_{EA} = V_B^2(N_i a) 4\pi^2 D_T \sigma^4 \exp[q_\perp^2 \sigma^2],$$

where  $V_{Bi}$  is the conduction band discontinuity at the interface located at the lattice site  $N_i$ . This model reduces to the widely used phenomenological model of Prange and Nee,<sup>30</sup>

$$\langle |C_{IR,i}(\mathbf{q}_\perp)|^2 \rangle_{EA} = V_B^2(N_i a) \pi \Lambda^2 \exp \left[ \frac{q_\perp^2 \Lambda^2}{4} \right]$$

if we use  $\Lambda = 2\sigma$  and  $D_T = 4/(\pi \Lambda^2) \simeq 1/(\Lambda^2)$ . This last identity is equivalent to assuming that the average separation between terraces is equal to the average terrace width. Similar identities are also given by Vinter and Weil.<sup>15</sup>

The coupling constant  $H_{IR,i}$  at the lattice site  $N_i$  obtained after integration of  $\langle |C_{IR,i}|^2 \rangle$  [see Eq. (19)] over the perpendicular momentum is

$$H_{IR,i}(E_{1x}) = \frac{V_{Bi}^2(N_i a)}{2} \Lambda^2 \frac{m^*}{\hbar^2} \times \exp \left[ -\frac{m^* \Lambda^2}{2\hbar^2} (E_0 - E_{1x} + E_{0L}) \right] \times I_0 \left[ \frac{m^*}{\hbar^2} \Lambda^2 (\sqrt{E_{0L}} \sqrt{E_0 - E_{1x}}) \right],$$

where  $I_0[x]$  is the modified Bessel function of order 0. Note that the terraces are usually one monolayer wide and  $a$  should be selected to be half a lattice parameter (the normal choice for the [100] direction<sup>18</sup>). Alternatively, if  $a$  is selected to be the lattice parameter,  $V_{Bi}$  should be divided by 4.

The last scattering process considered is alloy scattering (AL). In an alloy  $A_\alpha B_{1-\alpha}C$  the crystal potential is not periodic. However, the crystal potential of the alloy

can be represented in terms of a nonperiodic fluctuating potential superposed on an average potential which is periodic. This fluctuating potential introduces an effective scattering process referred to as alloy scattering. The coupling constant is<sup>31</sup>

$$\langle |C_{AL,i}(\mathbf{q}_\perp)|^2 \rangle_{EA} = \Delta V_{AB}^2 \alpha_i (1 - \alpha_i) \frac{\Omega^0}{a},$$

where  $\alpha_i$  is the mole fraction at the lattice site  $N_i$ ,  $\Omega^0$  is the volume of the elementary cell which is given in terms of the elementary crystal axis by  $\Omega^0 = a^3/4$ , and where  $\Delta V_{AB}$  is essentially the variation of the conduction band at  $\Gamma$  between alloy  $AC$  and  $BC$ . The coupling constant  $H_{AL,i}$  obtained after integration of  $\langle |C_{AL,i}|^2 \rangle_{EA}$  [see Eq. (19)] over the perpendicular momentum is

$$H_{AL,i}(E_{1x}) = \frac{1}{(2\pi)} \Delta V_{AB}^2 \alpha_i (1 - \alpha_i) \frac{\Omega^0}{a} \frac{m^*}{\hbar^2}.$$

## V. TRANSMISSION COEFFICIENT FOR PHONON-ASSISTED TUNNELING

Once the wave functions  $f_0$  and  $f_1$  have been obtained, one is then in a position to calculate the reflected or transmitted currents. We have demonstrated that for each electron of energy  $E_{0x}$  and perpendicular momentum  $\mathbf{k}_{10}$  incident on the superlattice we will obtain a continuous spectrum of scattered states of longitudinal energy  $E_{1x}$  and transversal energy  $E_{1L}$ . We are only interested in the average current obtained from an ensemble average over the scatterers. As discussed in the Appendix, when all the incident and scattered waves are assumed to be mutually uncorrelated, the total current is then directly given by the summation of the current carried by each of those states.

For simplicity we now limit the discussion to the tight-binding band. Let us introduce the amplitudes 1,  $b_0$ , and  $c_0$  of the incident, reflected, and transmitted wave  $f_0(n)$ ,

$$f_0(n) = \begin{cases} e^{ik_{0xL}na} + b_0 e^{-ik_{0xL}na} & \text{for } n < 0, \\ c_0 e^{ik_{0xR}na} & \text{for } n > L_{SL}/a = N_{SL}, \end{cases}$$

where the momentums  $k_{0xR}$  and  $k_{0xL}$  are obtained for a given energy  $E_{0x}$  from the tight-binding band structure of semiconductor  $L$  (left side) and  $R$  (right side)

$$E_{0x} = A_L - A_L \cos k_{0xL} a = A_R - A_R \cos k_{0xR} a.$$

Note that this last equation admits two solutions for both  $k_{0xL}$  and  $k_{0xR}$ . We assume here that  $A_L$  and  $A_R$  are positive numbers and select the positive values for  $k_{0xL}$  and  $k_{0xR}$ .

The incident and transmitted currents for the envelope function  $f_0$  are given, respectively, by

$$J_{I0}(E_{0x}) = ev_L(E_{0x}),$$

$$J_{T0}(E_{0x}) = e |c_0|^2 v_R(E_{0x}) = e |f_0(N_{SL})|^2 v_R(E_{0x}),$$

where  $v_L(E_{0x})$  is the velocity of semiconductor  $L$  on the left side of the superlattice and where  $v_R(E_{0x})$  is the ve-

locity of semiconductor  $R$  on the right side of the superlattice. Since we assume here that the regions  $L$  and  $R$  are flat, the electron velocity is simply given by

$$v_i(E_x) = \frac{1}{\hbar} \frac{d\mathcal{E}_i(k_x)}{dk_x}.$$

The transmitted current associated with the envelope function  $f_1$  is also given by  $e|c(E_{1x}, q_x)|^2 v_R(E_{1x})$ . The total average transmitted current  $J_{T,ph\pm}$  resulting from the emission or absorption of all the phonons is then given by

$$\begin{aligned} J_{T,ph\pm}(E_{0x}, E_{0l}) &= e \frac{1}{\Omega} \sum_{q_x > 0} \sum_{q_l} \langle C_{\pm}^2(\mathbf{q}) \rangle_{EA} |f_1(N_{SL}, E_{1x}, q_x)|^2 v_R(E_{1x}) \\ &= e \frac{1}{L_x} \sum_{q_x > 0} \int_{-2A_L}^{E_0 \pm \hbar\omega_{LO}} H_{\pm}(E_{1x}, E_{0l}, q_x) |f_1(N_{SL}, E_{1x}, q_x)|^2 v_R(E_{1x}) dE_{1x}. \end{aligned}$$

The total transmitted current  $J_{T,elast\pm}$  resulting from elastic scattering is similarly given by

$$\begin{aligned} J_{T,elast}(E_{0x}, E_{0l}) &= e \sum_i \frac{1}{S} \sum_{q_l} \langle |C_i(\mathbf{q}_l)|^2 \rangle_{EA} |f_1(N_{SL}, E_{1x}, i)|^2 v_R(E_{1x}) \\ &= e \sum_i \int_{-2A_L}^{E_0} H_i(E_{1x}, E_{0l}) |f_1(N_{SL}, E_{1x}, i)|^2 v_R(E_{1x}) dE_{1x}. \end{aligned}$$

The total forward transmission coefficient for an incident electron of longitudinal energy  $E_{0x}$  and perpendicular momentum  $\mathbf{k}_{0l}$  is then given by

$$T_F(E_{0x}, E_{0l}) = T_0 + T_{ph} + T_{elast}$$

using the elementary transmission coefficient

$$\begin{aligned} T_0(E_{0x}, E_{0l}) &= \frac{J_{T0}(E_{0x}, E_{0l})}{J_{I0}(E_{0x})}, \\ T_{ph}(E_{0x}, E_{0l}) &= \frac{J_{T,ph+}(E_{0x}, E_{0l}) + J_{T,ph-}(E_{0x}, E_{0l})}{J_{I0}(E_{0x})}, \\ T_{elast}(E_{0x}, E_{0l}) &= \frac{J_{T,elast}(E_{0x}, E_{0l})}{J_{I0}(E_{0x})}. \end{aligned}$$

A total reflection coefficient  $R_F$  can similarly be defined (by replacing  $N_{SL}$  by 0 and  $R$  by  $L$ ), and current conservation (see the Appendix) automatically enforces  $R_F + T_F = 1$ .

The total forward diode current per unit area from semiconductor  $L$  to  $R$  for a given Fermi energy  $E_{fL}$  on the left side (see Fig. 1) is then obtained by summing the transmitted current over all possible incident momenta  $\mathbf{k}_0$ ,

$$I_F(E_{fL}) = \frac{m^*}{2\pi^2 \hbar^2} \int_0^{2A_L} dE_{0x} \int_0^{2A_L} dE_{0l} \frac{e T_F(E_{0x}, E_{0l})}{\exp\left[\frac{E_0 - E_{fL}}{k_B T_0}\right] + 1} \quad (23)$$

with  $E_0 = E_{0x} + E_{0l}$ .

The total backward diode current  $I_B$  per unit area from semiconductor  $R$  to  $L$  for a given Fermi energy  $E_{fR}$  on the right side is obtained from the same equation by switching the direction of the Hamiltonian and the indices  $R$  and  $L$ . The total diode current  $I$  per unit area is given by the difference between the forward and backward current  $I = I_F(E_{fL}) - I_B(E_{fR})$ .

## VI. NUMERICAL SOLUTION

The ensemble average solution of the Schrödinger equation in the presence of phase-breaking scattering has reduced to the solution of a set of coupled difference equations. The coupling involves an integration over a continuum of energy  $E_{1x}$ . For the numerical calculation

we replace this integration over  $E_{1x}$  by a summation over a discrete set of energies  $E_{1x,r}$ . For this purpose we use the Simpson integration rule generalized to inequally spaced energy levels  $E_{1x,r}$ . The critical part of this numerical integration is the determination of the energies  $E_{1x,r}$ . We have developed an integration algorithm, based on the Simpson integration rules, which estimates the integration error and introduces new energies  $E_{1x,r}$  where most necessary, so as to achieve the desired target integration error. An initial scanning of the energy with a resolution specified by the user is used to detect any fine structures. For the 50/50/50 test diode studied here a 1-meV initial scanning resolution is sufficient to detect all the fine structures of the scattering-assisted tunneling process. The number  $N_r$  of energies used for the calculation therefore includes the initial scanning energy points



plus the ones introduced by the algorithm. For the test diode simulation reported below an average of 200 energies  $E_{1x,r}$  is typical for a single scattering process.

The solution of the Schrödinger equation in the presence of scattering therefore reduces to the solution of the difference equation (15) coupled to a finite set of difference equations (16) and (17). For phonon scattering the number of difference equations (16) is  $N_q \times N_r$  where  $N_q$  is the number of phonon modes  $q_x$ . To reduce the size of the system to be solved we limited the solution to the first (odd)  $N_{SL} = L_{SL}/a$  phonon modes  $q_x$ . Only the odd modes contribute since the odd modes can be approximated by 1 ( $\sin q_x a \simeq 1$ ) in the superlattice region and the even modes approximated by 0 for small values of  $q_x$ . For polar scattering the higher phonon modes were verified to be negligible both because of the  $1/q$  weight in the phonon-electron interaction and the fast variation of the standing wave  $\sin(q_x a)$  which seems to provide a phase cancellation suppressing phonon scattering. As a result, for the first  $N_{SL}$  modes we have effectively  $N_q = 1$ , and the size of the system is much reduced.

An exact numerical solution of Eqs. (15), (16), and (17) can be easily obtained since this is a system of linear

equations. The solution of  $N_r + 1$  coupled difference equations with the boundary conditions given above can be reduced using the difference equations to the solution of a linear system of  $2N_r + 2$  equations and unknowns. Indeed in addition to  $b_0$ ,  $c_0$ , we have  $N_r$  unknown coefficients  $b_r$  and  $c_r$ . For several scattering mechanisms the size of this system grows rapidly and the calculation becomes too slow.

A more efficient method consists of first calculating the coupling terms  $G(n)$ . Indeed as one can expect from a linear system the functions  $f_1(n)$  can be expressed as

$$f_1(n) = \sum_{i=1}^{N_{SL}} h_i(n) f_0(i),$$

where the function  $h_i(n)$  is the impulse response solution of Eq. (17) with  $f_0(n) = 1$ . Substituting  $f_1(n)$  in Eq. (16) or (17) we find that the coupling terms  $G(n)$  can be written

$$G(n) = \sum_{i=1}^{N_{SL}} H_{SE}(n, i) f_0(i),$$

where we have for phonon scattering

$$H_{SE,\pm}(n, i, q_x) = \sin(q_x n a) \int_{-2A_L}^{E_0 \pm \hbar\omega(q_x)} h_i(n, E_{1x}) H_{\pm}(E_{1x}, q_x) dE_{1x}$$

and for elastic scattering

$$H_{SE}(n, i) = \delta_{nN_i} \int_{-2A_L}^{E_0} h_i(n, E_{1x}) H_i(E_{1x}) dE_{1x}.$$

$H_{SE}$  is the so-called self-energy matrix. This is a complex non-Hermitian matrix. The real part of the self-energy matrix shifts the resonant energy of the double barrier. The imaginary part accounts for the loss of current of the incident wave  $f_0(n)$  by scattering. Note that the global current conservation ( $R_F + T_F = 1$ ) is independent of the energies  $E_{1x,r}$  used. Current conservation (see the Appendix) is always found to be numerically enforced up to the last digit. The incident wave  $f_0(n)$  is then obtained by solving a small system of  $N_{SL}$  unknowns with  $N_{SL}$  equations. The advantage of this method is that the impulse response calculated can be used for all incident electrons of energy  $E_{0x}$  sharing the same transversal energy  $E_{01}$ . For the 50/50/50 test device considered this approach reduces the calculation time by a factor of 40. This approach permits us to handle multiple sequential scattering in an iterative fashion (see discussion in Sec. VIII).

The complete phonon-assisted tunneling algorithm developed is controlled by a single error: the desired target error for the current being calculated. The error control algorithm developed for this purpose guarantees that the targeted error is met and that the integration calculation is efficient and fast.

The algorithm was written in FORTRAN. The calculations were performed with the Ohio Cray Y-MP. A SUN 3 was used as a terminal. The calculation of one  $I$ - $V$

point for an error of 1% in the total current for the resonant tunneling diode discussed below was found to require on average the calculation of 2000 transmission coefficients taking on average 3 min of Cray time. An  $I$ - $V$  characteristic (20 points) takes therefore one Cray hour.

## VII. NUMERICAL RESULTS

In this section we first analyze the individual impact of polar, acoustic, alloy, and interface roughness scattering mechanisms upon resonant tunneling before considering their combined effect.

Let us start by polar scattering. We show in Figs. 2(a) and 2(b) the equilibrium (no bias) transmission coefficient  $T_F(E_{0x}, E_{01})$  plotted versus  $E_{0x}$  for  $E_{01} = 0$  for a 34/34/34- and 50/50/50-Å diode at the lattice temperature of 4.2 K (dashed line), 100 K (dashed-dotted line), and 300 K (dotted line). Also shown is the transmission coefficient in the absence of scattering (solid line).

Three different transmission peaks are observed. Indeed the transmission coefficient plotted is the superposition of direct tunneling and phonon-assisted tunneling by emission and absorption of optical phonons. The main peak centered upon the energy  $E_{res} \simeq 86.1$  meV corresponds to direct resonant tunneling  $T_0$  by unscattered electrons. Note the 3.5-meV self-energy shift of the main resonant transmission peak relative to the one obtained in the absence of scattering  $E_{res,0} \simeq 89.6$  meV. The right peak centered upon  $E_{res,0} + \hbar\omega_{LO}$  corresponds to resonant tunneling assisted by emission of phonons. The left peak

centered upon  $E_{\text{res},0} - \hbar\omega_{\text{LO}}$  corresponds to resonant tunneling assisted by absorption of phonons. This absorption peak cannot be observed at low temperature (4.2 K) due to the small phonon population. Our simulator (not the model) is presently limited to a single sequential scattering event for phonons. The presence of a second phonon scattering would also introduce a self-energy shift for these secondary transmission peaks.

In general the higher the temperature the higher the phonon-assisted tunneling peaks. Note that at 300 K the main peak of the transmission coefficient of the 50/50/50-Å diode [Fig. 2(b)] is considerably more broadened than that of the 34/34/34-Å diode [Fig. 2(a)]. This is due to the fact that the resonant tunneling peak in the 50/50/50 diode is much sharper (a fraction of meV wide), which permits us to resolve the large 3D broadening induced by polar scattering at room temperature. Such a result cannot be predicted if the transversal momentum is assumed to be constant (one-dimensional model).

This is not, however, the only possible source of three-dimensional broadening. In Fig. 3 we show the equilibrium (no bias) transmission coefficient  $T_F(E_{0x}, E_{0l})$  plotted

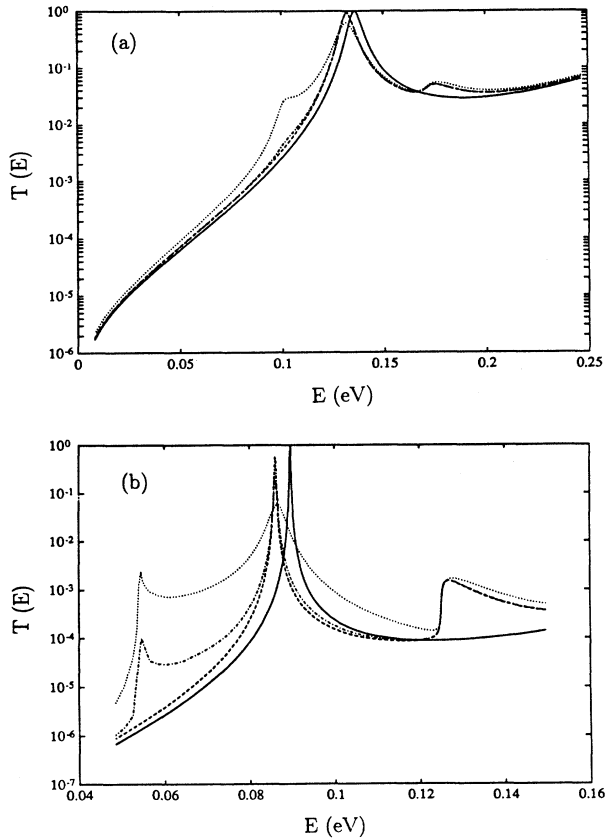


FIG. 2. Equilibrium (no bias) transmission coefficient  $T_F(E_{0x}, E_{0l}=0)$  vs  $E_{0x}$  in the presence of polar scattering for an (a) 34/34/34- and (b) 50/50/50-Å diode at the lattice temperature of 4.2 K (dashed line), 100 K (dashed-dotted line), and 300 K (dotted line). Also shown is the transmission coefficient in the absence of polar scattering (solid line).

versus  $E_{0x}$  for various perpendicular energies  $E_{0l}$  at 100 K (4.2 K is very similar). The main peak of the transmission coefficient is the highest when  $E_{0l}$  is 0 (solid line) and rapidly reduces for 0.05 eV (dashed line) before increasing again for 0.1 eV (dashed-dotted line) and 0.15 eV (dotted line). Secondary peaks in the transmission coefficient corresponding to emission (4.2 and 100 K) and absorption (100 K) of phonons can only be distinctly observed for incident electrons with very small perpendicular momentum  $E_{0l} \approx 0$ . Notice that the peak of the transmission coefficient is also shifting with the perpendicular momentum. This shift is the major source of broadening at lower temperature.

Let us now examine the impact of polar scattering upon the  $I$ - $V$  characteristic of a 34-Å barrier diode. The  $I$ - $V$  characteristic calculated for a 34/34/34-Å diode in the presence (dashed line) and absence (solid line) of polar scattering at 4.2 and 100 K is shown in Figs. 4(a) and 4(b). As we can see the peak current is decreased and the valley current is increased in the presence of polar scattering. Polar scattering therefore contributes to the reduction of the peak to valley current ratio. At 4.2 K the phonon emission peak of the transmission coefficient has introduced a secondary peak in the  $I$ - $V$  characteristic around  $V_D = 0.6$  V. In Fig. 5 we show the larger transmission coefficient resulting at  $V_D = 0.6$  V in the presence of phonon-assisted tunneling at 4.2 and 100 K (solid line, not distinguishable) compared to the transmission coefficient obtained in the absence of polar scattering (dashed line). At a higher temperature (100 K) such a secondary peak cannot usually be observed because the phonon-assisted current is small compared to the total diode current. Indeed the diode current is approximately proportional to the area under the transmission coefficient from 0 to the Fermi energy  $E_{fc}$  which is 11.47 and 82 meV at 4.2 and 100 K, respectively.

Similar effects are also observed in the 50-Å barrier diode at 4.2 and 100 K. Let us consider, however, the 300 K  $I$ - $V$  characteristic shown in Fig. 6. The large broadening introduced by phonon scattering at 300 K

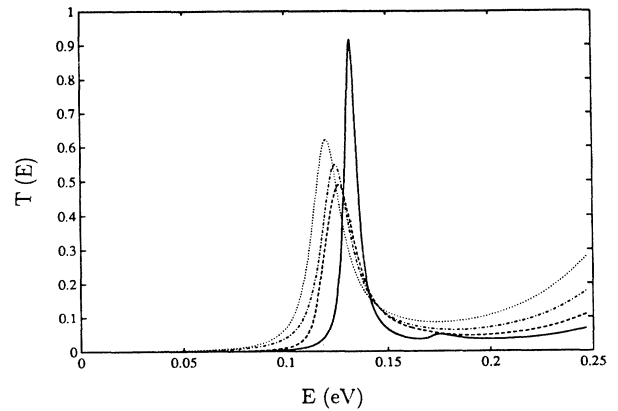


FIG. 3. Plots of the 100-K equilibrium ( $V_D = 0$ ) transmission coefficient  $T_F(E_{0x}, E_{0l})$  vs  $E_{0x}$  for the perpendicular energies  $E_{0l}$  of 0 eV (solid line), 0.05 eV (dashed line), 0.1 eV (dashed-dotted line), and 0.15 eV (dotted line).

[see Fig. 2(b)] has now completely removed the negative conductance region in the diode  $I$ - $V$  characteristic. This demonstrates the importance of a 3D analysis which accounts for the variation of the perpendicular momentum.

Next let us consider the impact of acoustic phonons upon the transmission coefficient. We show in Figs. 7(a) and 7(b) the equilibrium (no bias) transmission coefficient  $T_F(E_{0x}, E_{0l})$  plotted versus  $E_{0x}$  for  $E_{0l}=0$  for 34/34/34- and 50/50/50-Å diode at the lattice temperature of 4.2 K (dotted line), 100 K (dashed-dotted line), and 300 K (dashed line). Also shown is the transmission coefficient in the absence of scattering (solid line). Compared to polar scattering the impact of acoustic scattering upon resonant tunneling is small. The maximum self-energy shift at 300 K is 2.7 and 3 meV for the 34- and 50-Å diode, respectively. Note that two different transmission peaks are observed for the 50-Å diode corresponding to direct tunneling and phonon-assisted tunneling by emission and absorption of acoustic phonons. This splitting is, however, an artifact which would be suppressed if a second sequential scattering event were introduced. Indeed the self-energy introduced by the secondary transmission peak would shift it so that both peaks would merge in a single one, as in the 34-Å diode. As expected, the impact of the acoustic phonon on the  $I$ - $V$  characteristic shown in

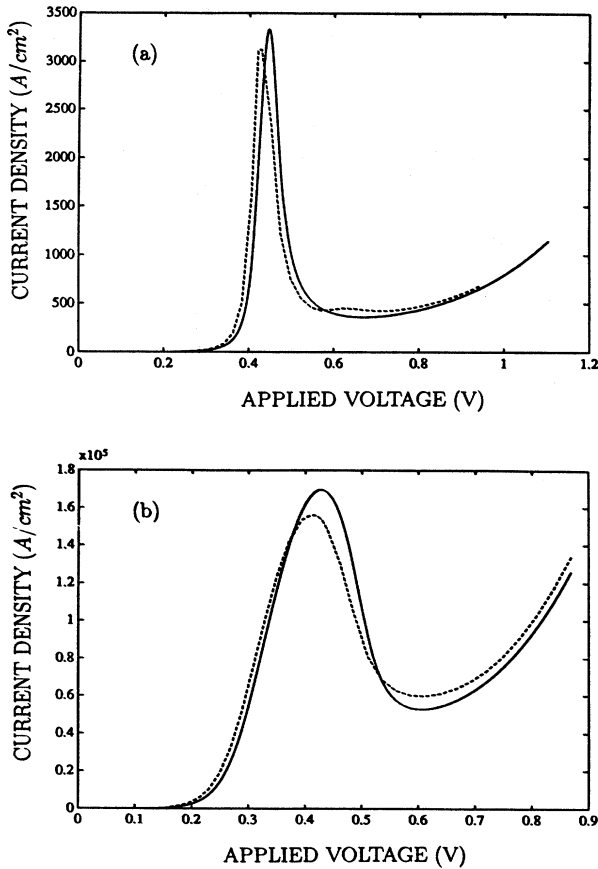


FIG. 4.  $I$ - $V$  characteristic in the presence (dashed line) and absence (solid line) of polar scattering calculated for a 34/34/34-Å diode at (a) 4.2 and (b) 100 K.

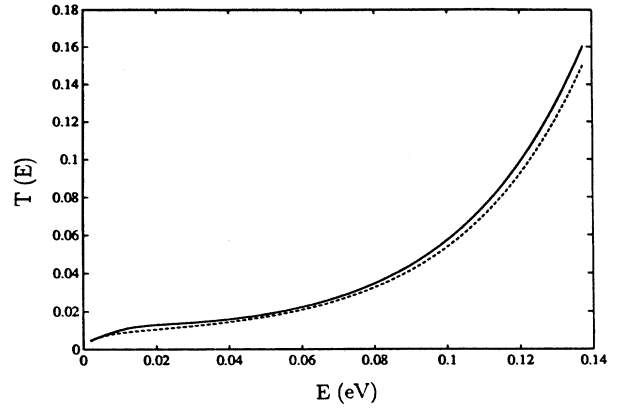


FIG. 5. Transmission coefficient  $T_F$  resulting at  $V_D=0.6$  V for a 34/34/34-Å diode in the presence of phonon-assisted tunneling at 4.2 (solid line) and 100 K (dotted line, not distinguishable from the solid line) compared to the transmission coefficient obtained in the absence of scattering (dashed line).

Fig. 8 is seen to be negligible. These  $I$ - $V$  data tend to indicate that the development of a more accurate model of acoustic scattering (the elastic approximation was used here) is not necessary for resonant tunneling.

Let us now consider interface roughness scattering. We show in Figs. 9(a) and 9(b) the equilibrium (no bias) transmission coefficient  $T_F(E_{0x}, E_{0l})$  plotted versus  $E_{0x}$  for  $E_{0l}=0$  for a 34/34/34- (and 50/50/50-Å) diode for 0, 1, 3, and 6/20 sequential scattering events. Note that this scattering mechanism is temperature independent. The average terrace size used is  $\Lambda=70$  Å. One clearly sees that the transmission coefficient converges after a few sequential 3D scattering events (6 for the 34-Å diode and 20 for the 50-Å diode). The importance of interface roughness scattering is measured by the large self-energy shift (about 11 meV for the 34-Å diode and 7 meV for the 50-Å diode). Note the resulting *asymmetric* shape of the transmission coefficient after several sequential scattering events. As a consequence, the valley current will be

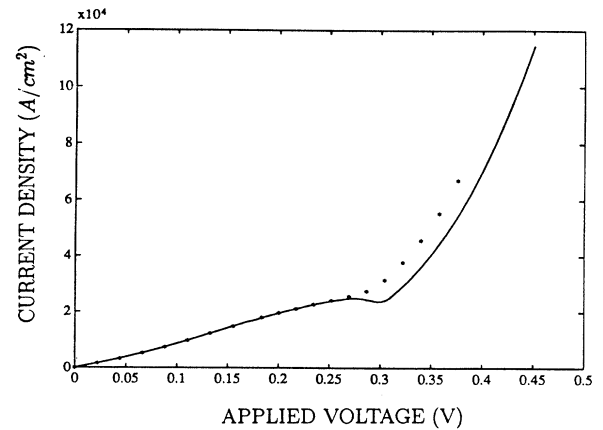


FIG. 6.  $I$ - $V$  characteristic in the presence (star) and absence (solid line) of polar scattering calculated for a 50/50/50-Å diode at 300 K.

strongly increased due to the slow decrease of the transmission coefficient at large energies. However, the peak current is not much affected because the total area under the transmission coefficient does not vary. The resulting current voltage characteristic confirming these predictions is shown in Fig. 10. This figure shows the current voltage characteristic after 0,1,2 sequential IR scattering events at 100 K. As we can see convergence occurs much faster than for the transmission coefficient. This is due to the fact that the current is relatively insensitive to the high frequency variation of the transmission coefficient but is proportional to the area under the transmission coefficient. These simulations support the concept that the interface quality is of prime importance to control the valley current. Note that we have assumed in the ensemble average performed [see Eq. (12)] that interface roughness scattering events by different interfaces were uncorrelated. A weak (two bodies) correlation could easily be included in the present model. The correlation of such interface scattering events, if important, could lead to additional structures (weak localization) in the transmission coefficient. Henrickson *et al.*<sup>32</sup> have shown that this can lead to a splitting of the resonant

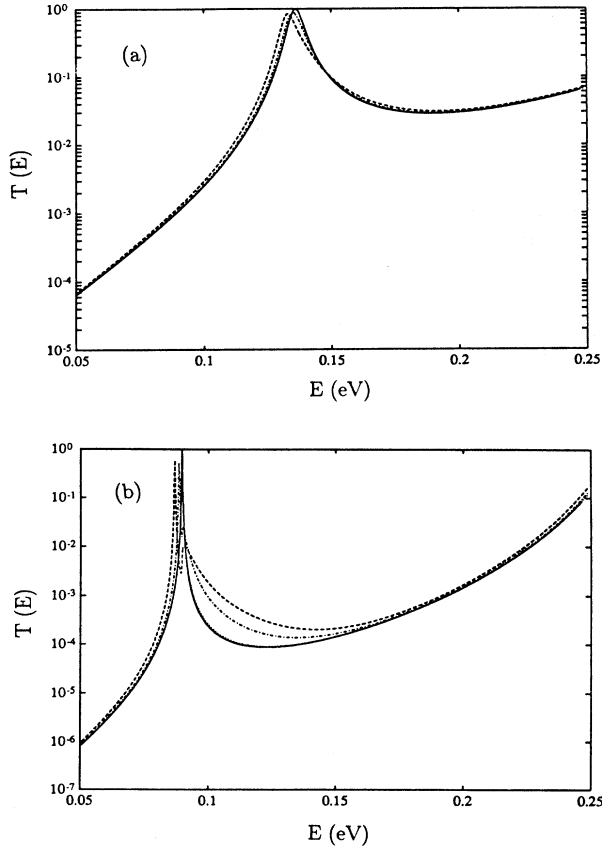


FIG. 7. Equilibrium (no bias) transmission coefficient  $T_F(E_{0x}, E_{0l}=0)$  vs  $E_{0x}$  in the presence of acoustic scattering for (a) 34/34/34- and (b) 50/50/50-Å diode at the lattice temperature of 4.2 K (dotted line), 100 K (dashed-dotted line), and 300 K (dashed line). Also shown is the transmission coefficient in the absence of scattering (solid line).

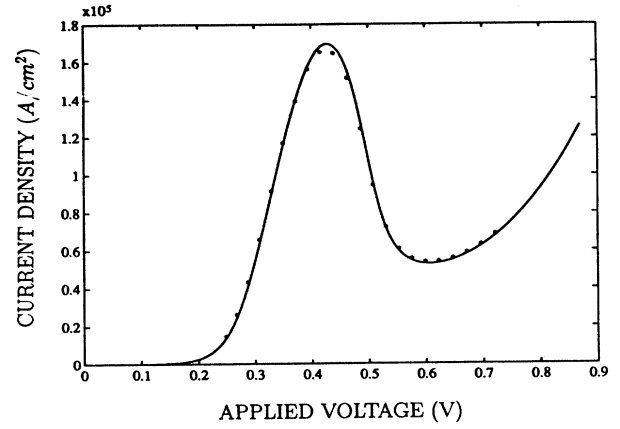


FIG. 8.  $I-V$  characteristic in the presence (star) and absence (solid line) of acoustic scattering calculated for an 34/34/34-Å diode at 100 K. The impact of acoustic scattering on the  $I-V$  characteristic at 100 K for a 34/34/34-Å diode.

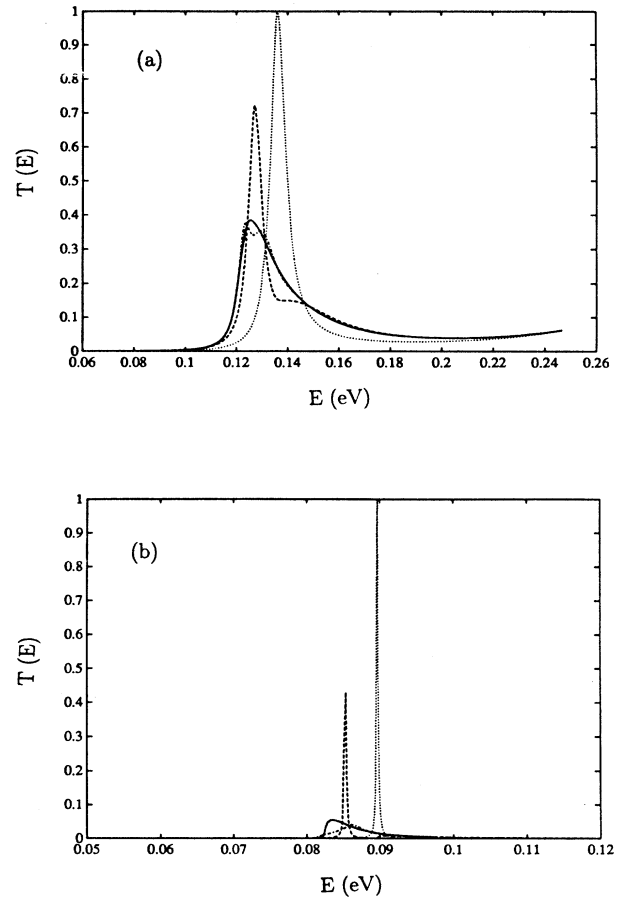


FIG. 9. Equilibrium (no bias) transmission coefficient  $T_F(E_{0x}, E_{0l}=0)$  vs  $E_{0x}$  in the presence of interface roughness scattering for an (a) 34/34/34- and (b) 50/50/50-Å diode for 0 (dotted line), 1 (dashed line), 3 (dashed-dotted line), and 6 (34-Å diode) and 20 (50-Å diode) sequential scattering events.

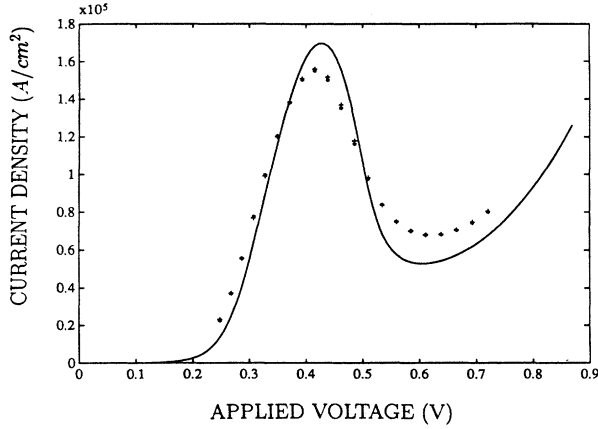


FIG. 10. Current voltage characteristic of a 34/34/34-Å diode at 100 K after 0 (solid line), 1 (\*), and 2 (+) sequential IR scattering events.

peak in double-barrier structures with a very thin well (20 Å) and high barriers.

Finally, let us consider alloy scattering. We show in Fig. 11 the equilibrium (no bias) transmission coefficient  $T_F(E_{0x}, E_{0l})$  plotted versus  $E_{0x}$  for  $E_{0l}=0$  for a

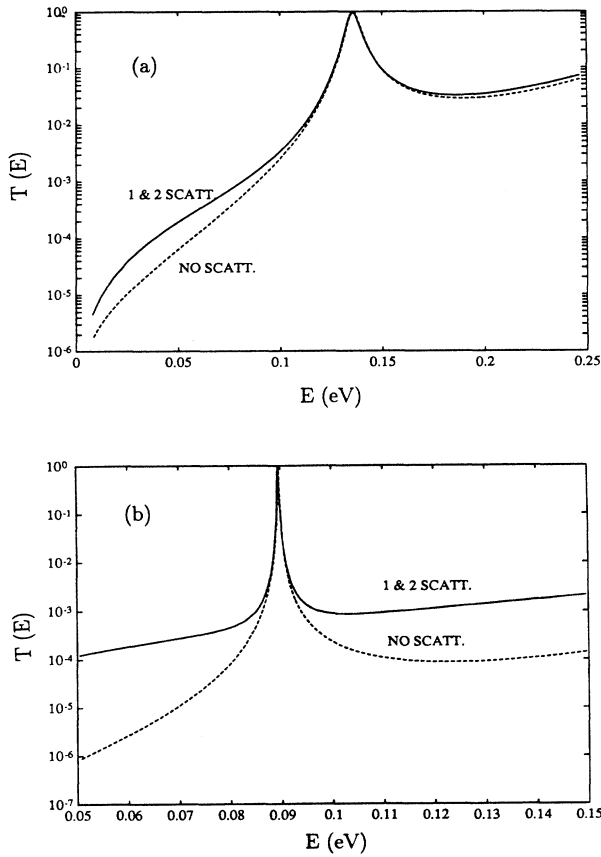


FIG. 11. Equilibrium (no bias) transmission coefficient  $T_F(E_{0x}, E_{0l}=0)$  vs  $E_{0x}$  in the presence of alloy scattering for an (a) 34/34/34- and (b) 50/50/50-Å diode for 0 (dashed line), 1 (solid line), and 2 (dotted line, not distinguishable from 1) sequential scattering events.

34/34/34- (and 50/50/50-Å) diode for 0, 1, and 2 sequential scattering events. It is not possible to distinguish the 1 and 2 sequential scattering events in Fig. 11. Clearly this indicates that only one single sequential scattering event is necessary for alloy scattering. The impact upon the  $I$ - $V$  characteristic at 100 K shown in Fig. 12 is small.

We now consider the combined impact upon resonant tunneling of these four scattering mechanisms. We show in Figs. 13(a) and 13(b) the equilibrium (no bias) transmission coefficient  $T_F(E_{0x}, E_{0l})$  plotted versus  $E_{0x}$  for  $E_{0l}=0$  for a 34/34/34- and 50/50/50-Å diode at the lattice temperature of 4.2, 100, and 300 K. Also shown is the transmission coefficient in the absence of scattering. Clearly the transmission coefficient exhibits complex structures resulting from the superposition of each scattering mechanism. However, one can recognize the dominant contribution of both polar (LO) and interface roughness (IR) scattering. To emphasize the interaction between these scattering mechanisms resulting from backscattering, we show in Fig. 14 the various transmission coefficients  $T_0$ ,  $T_{IR}$ ,  $T_{AC+LO}$ , and  $T_{al}$  which contribute to the total transmission coefficient at 100 K. One can verify that a structure present at an energy in a given transmission coefficient (e.g., a peak in  $T_{AC+LO}$ ) induces antistuctures at the same energy in the other transmission coefficients.

The current voltage characteristic obtained for the 34/34/34- and 50/50/50-Å diodes at 100 K is shown in Fig. 15. To save computer resources, a constant mass was used, and the average over the perpendicular energy was performed analytically for the 50-Å barrier diode. The various scattering mechanisms (dominated here by IR) merely cooperate to reduce the peak to valley current ratio of the diode. It is interesting to note that the complicated structures present in the transmission coefficient are not resolved in the  $I$ - $V$  characteristic at 100 K. However, a notable exception was the 4.2 K  $I$ - $V$  characteristic of Fig. 4(a) in which phonon-assisted tunneling induced a bump in the  $I$ - $V$  characteristic.

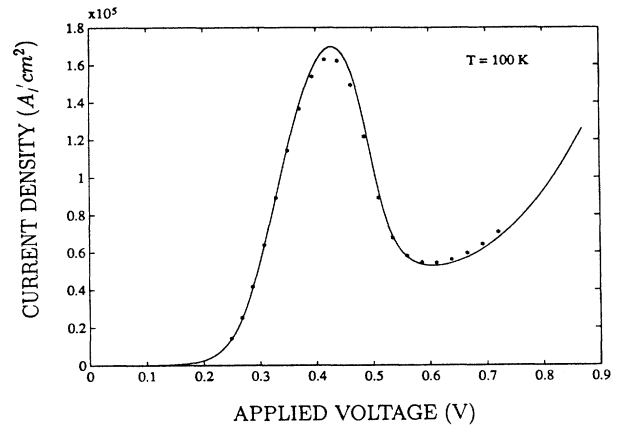


FIG. 12.  $I$ - $V$  characteristic in the presence (solid line) and absence (star) of alloy scattering calculated for a 34/34/34-Å diode at 100 K.

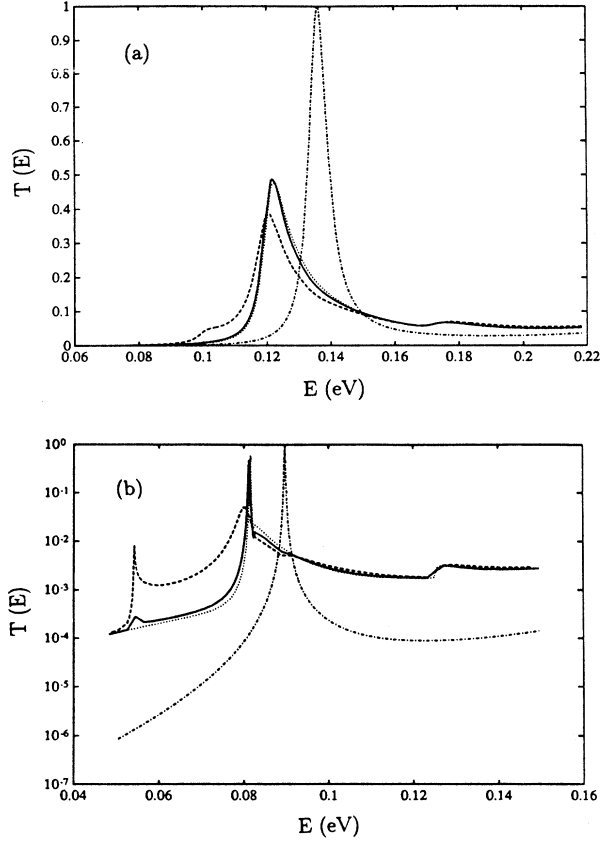


FIG. 13. Equilibrium (no bias) transmission coefficient  $T_F(E_{0x}, E_{0l}=0)$  vs  $E_{0x}$  for  $E_{0l}=0$  in the presence of LO, ac, IR, and al scattering for an (a) 34/34/34-Å and (b) 50/50/50-Å diode at the lattice temperature of 4.2 K (dotted line), 100 K (solid line), and 300 K (dashed line). Also shown is the transmission coefficient in the absence of scattering (dotted-dashed line).

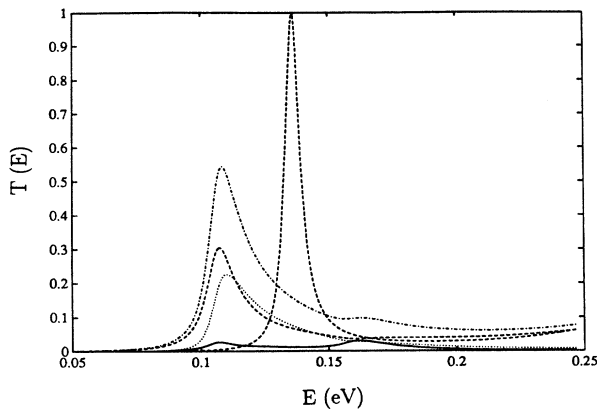


FIG. 14. Equilibrium (no bias) transmission coefficient  $T_F$  (dashed line),  $T_O$  (dashed line),  $T_{IR}$  (dotted line),  $T_{ac+LO}$  (solid line), and  $T_{AL}$  (dotted line, too small to be distinguished) vs  $E_{0x}$  for  $E_{0l}=0$  for a 34/34/34-Å diode at the lattice temperature of 100 K. Also shown is the transmission coefficient in the absence of scattering (dashed line reaching 1 at resonance).

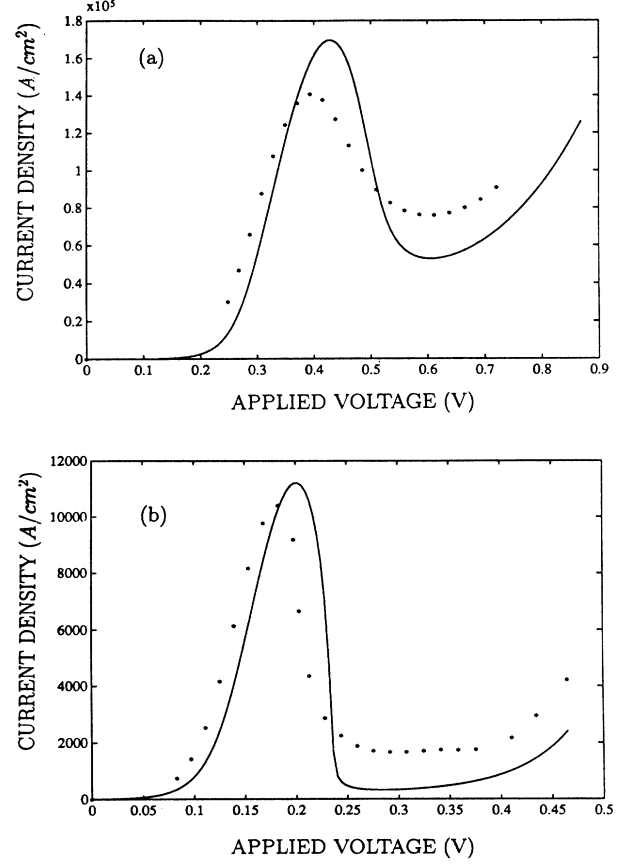


FIG. 15. Current voltage characteristic obtained for the (a) 34/34/34- and (b) 50/50/50-Å diodes at 100 K in the presence of LO, ac, IR, and al scattering (stars) and in the absence of scattering (solid line).

## VIII. CONCLUSION

In this paper we presented a 3D model and simulator of scattering-assisted tunneling for finite length heterostructures. This quantum simulator solves the Schrödinger equation in 3D using a sequential scattering event expansion. The wave function and transmission and reflected currents are calculated using an (analytic) ensemble average over the scatterers which assume that the sequential scattering events are uncorrelated. The sequential scattering event expansion used includes back-scattering so that current conservation is enforced (a regular perturbative treatment does not). This model admits an exact numerical solution based on the solution of a large system of linear equations.

Multiple sequential scattering was implemented for alloy scattering and interface roughness scattering. The quantum simulator uses a backward iterative numerical algorithm to handle multiple scattering, which avoids duplication of calculation. Indeed a direct forward approach for  $N$  sequential scattering events (at a single lattice site  $N_i$ ) would require solving a system of at least  $300^N$  Schrödinger equations since  $300^N$  scattered waves are generated at the  $N$ th scattering event, assuming a single 3D scattering event can be accurately mapped by 300

outgoing scattered waves. Instead, the backward iterative algorithm used only requires a computation time proportional to the number of multiple sequential events  $N$  (i.e., the Schrödinger equation is solved  $300 \times N$  in the sample considered).

Note also that the Wannier picture used can handle more complete band-structures without much increase in computation time (see Ref. 22 for a demonstration showing a special  $\Gamma$  to  $X$  resonance in the double-barrier diode).

This scattering-assisted tunneling simulator was applied to two double-barrier structures. Polar scattering and interface roughness scattering were the dominant scattering mechanisms in the devices studied. Multiple sequential scattering was shown to lead to transmission coefficients versus energy with a characteristic peaked shape, which increase the valley current of the diode  $I$ - $V$  current characteristic. The three-dimensional treatment of the phonon-scattering processes featured by this model introduces an effective broadening of the transmission coefficient [see Figs. 2(b) and 3] particularly at 300 K which cannot be predicted by a one-dimensional model (e.g., Ref. 10). The broadening introduced by polar scattering was shown to contribute to the reduction of the peak to valley ratio of the  $I$ - $V$  characteristic and even suppress the negative conductance at room temperature (see Fig. 6).

This scattering-assisted tunneling simulator could be useful for testing other quantum device structures such as the Bloch oscillator<sup>2,5</sup> and the Zener oscillator.<sup>3</sup> For these longer devices, multiple sequential events of phonon scattering are expected to become important.

#### ACKNOWLEDGMENTS

This work was made possible thanks to grants from the CRAY corporation and the support of the Ohio State University. The computer time on the CRAY Y-MP was provided by a grant from the Ohio Supercomputer Center. The authors would like to thank Furrukh Khan and Bruce Patton (The Ohio State University), Bob Potter (Applied Signal), Borge Vinter and François Chevoir (Thomson-CSF), Abul Khonker (Clarkson University), and John Davies (Glasgow University) for fruitful discussions about resonant tunneling.

#### APPENDIX: CURRENT CONSERVATION

The current  $J(n)$  at the site  $n$  is obtained from the sum of the elemental currents  $j(n, n')$  (see Ref. 22 generalized here to 3D),

$$J(n) = \int \int_{-\pi/a}^{\pi/a} \left\{ \sum_{m=1}^N \sum_{p=0}^{m-1} j(n-p, n-p+m, \mathbf{k}_\perp) + j(n+p-m, n+p, \mathbf{k}_\perp) \right\} d\mathbf{k}_\perp, \quad (\text{A1})$$

where  $j(n, n', \mathbf{k}_\perp)$  is the elemental electron current (see Ref. 22) from the lattice site  $n$  to the lattice site  $n'$  for the state  $i$  (0 or 1r) given by

$$j(n, n', \mathbf{k}_\perp) = e(-a/\hbar) \text{Im} \{ H_{nn'} f^*(n, \mathbf{k}_\perp) f(n', \mathbf{k}_\perp) \}.$$

For the tight-binding case  $J(n)$  simply reduces to elemental currents entering and leaving the site  $n$ ,

$$J(n) = \int \int_{-\pi/a}^{\pi/a} \{ j(n, n+1, \mathbf{k}_\perp) + j(n-1, n, \mathbf{k}_\perp) \} d\mathbf{k}_\perp. \quad (\text{A2})$$

To calculate the total current for the scattering-assisted tunneling problem we replace the envelope  $f(n, \mathbf{k}_\perp, t)$  of Eq. (14) in Eq. (A1) and perform an ensemble average over the scatterers.

Using our assumption that the scattering events are mutually uncorrelated, we obtain the simple result that the total current is the sum of the current  $J_i(n)$  supported by each energy state  $i$ ,

$$\langle J(n) \rangle_{\text{EA}} = J_0 + \sum_r J_{1r},$$

where the label  $J_0$  is the current of the incident state and  $J_{1r}$  the current of the scattered state  $1r$ . The summation over  $r$  is carried over all the scattered states.

Note that the current  $J_i$  or electron velocity  $v_i$  supported by the state  $i$  is obtained from the sum of the elemental currents  $j_i(n, n')$  (see Ref. 22),

$$\begin{aligned} J_i(n) &= e |f_i(n)|^2 v_i(n) \\ &= \sum_{m=1}^N \sum_{p=0}^{m-1} j_i(n-p, n-p+m) \\ &\quad + j_i(n+p-m, n+p), \end{aligned} \quad (\text{A3})$$

which for the tight-binding case  $J_i(n)$  simply reduces to elemental currents entering and leaving the site  $n$ ,

$$J_i(n) = e |f_i(n)|^2 v_i(n) = j_i(n, n+1) + j_i(n-1, n), \quad (\text{A4})$$

where  $j_i(n, n')$  is the elemental electron current (see Ref. 22) from the lattice site  $n$  to the lattice site  $n'$  for the state  $i$  (0 or 1r) given by

$$j_i(n, n') = e(-a/\hbar) \text{Im} \{ H_{nn'} f_i^*(n) f_i(n') \}. \quad (\text{A5})$$

Having defined the current, let us demonstrate that the current is conserved. Using the Wannier picture, scattering-assisted tunneling was shown to reduce to the solution of a set of coupled difference equations which for uncorrelated scattering events is given by Eqs. (15) and (16) or (17). Note that the coupling involves an integration over a continuum of energy  $E_{1x}$  which we replaced by a summation over a discrete set of  $E_{1x,r}$ . This system of equations can be rewritten in the form

$$E_{0x} f_0(n) = \sum_{n'} H_{nn'} f_0(n') + \sum_r C_r(n) f_{1r}(n), \quad (\text{A6})$$

$$E_{1x,r} f_{1r}(n) = \sum_{n'} H_{nn'} f_{1r}(n') + C_r^*(n) f_0(n), \quad (\text{A7})$$

where  $C_r(n)$  is the coupling constant.

Multiplying Eqs. (A6) and (A7) by  $f_0^*(n)$  and by  $f_{1r}^*(n)$ , respectively, and taking the imaginary part gives the following elemental current conservation equations:

$$\begin{aligned}
 0 &= \sum_{n'} j_{0,n,n'} + \sum_r j_{0,1r}(n) , \\
 0 &= \sum_{n'} j_{1r,n,n'} + j_{1r,0}(n) ,
 \end{aligned}
 \tag{A8}$$

where  $j_i(n, n')$  is the elemental electron current from the lattice site  $n$  to the lattice site  $n'$  for the state  $i$  (0 or 1r) given by Eq. (A5) and where  $j_{0,1r}(n)$  is the electron current from the state 0 to 1r and  $j_{1r,0}(n)$  from state 1r to 0 (both at the lattice site  $n$ ) defined by

$$j_{0,1r}(n) = e(-a/\hbar) \text{Im} \{ C_r(n) f_0^*(n) f_{1r}(n) \} ,$$

$$j_{1r,0}(n) = e(-a/\hbar) \text{Im} \{ C_r^*(n) f_{1r}^*(n) f_0(n) \} .$$

The latter interstate currents verify  $j_{0,1r}(n) = -j_{1r,0}(n)$ . This property enforces the conservation of the elemental electron currents. The conservation of the total electron current  $J(n)$  follows from it. Indeed the total current  $\langle J(n) \rangle_{\text{EA}}$  at a site  $n$  is obtained from a summation of elemental currents (A3). The conservation of the elemental currents expressed by Eqs. (A8) and the elemental current property  $j_j(n, m) = -j_i(m, n)$  therefore guarantees the conservation of the total current from site to site.

- 
- <sup>1</sup>L. L. Chang, L. Esaki, and R. Tsu, *Appl. Phys. Lett.* **24**, 593 (1974).  
<sup>2</sup>L. Esaki and R. Tsu, *IBM J. Res.* **14**, 61 (1970).  
<sup>3</sup>P. Roblin and M. W. Muller, *Semicond. Sci. Technol.* **1**, 218 (1986).  
<sup>4</sup>T. C. L. G. Sollner, W. D. Goodhue, P. E. Tannenwald, C. D. Parker, and D. D. Peck, *Appl. Phys. Lett.* **43**, 588 (1983).  
<sup>5</sup>A. Sibille, J. F. Palmier, and H. Wang, *Phys. Rev. Lett.* **64**, 52 (1990).  
<sup>6</sup>F. Beltram, F. Capasso, D. Sivco, A. L. Hutchinson, S. N. G. Chu, and A. Y. Cho, *Phys. Rev. Lett.* **64**, 3167 (1990).  
<sup>7</sup>F. Chevoir and B. Vinter (unpublished).  
<sup>8</sup>W. R. Frensley, *Phys. Rev. B* **26**, 1570 (1987).  
<sup>9</sup>K. L. Jensen and F. A. Buot, *J. Appl. Phys.* **67**, 7602 (1990).  
<sup>10</sup>N. S. Wingreen, K. W. Jacobsen, and J. W. Wilkins, *Phys. Rev. Lett.* **61**, 1396 (1988).  
<sup>11</sup>J. Leo and A. H. MacDonald, *Phys. Rev. Lett.* **64**, 817 (1990).  
<sup>12</sup>S. Datta, *Phys. Condens. Matter* **2**, 8023 (1990).  
<sup>13</sup>V. J. Goldman, D. C. Tsui, and J. E. Cunningham, *Phys. Rev. B* **36**, 7635 (1987).  
<sup>14</sup>A. D. Stone and P. A. Lee, *Phys. Rev. Lett.* **54**, 1196 (1985).  
<sup>15</sup>B. Vinter and T. Weil, *Superlatt. Microstruct.* **3** (1987).  
<sup>16</sup>H. Mizuta, T. Tanoue, and S. Takahashi, *Theoretical Analysis of Peak-to-Valley Ratio Degradation caused by Scattering Processes in Multi-Barrier Resonant Tunneling Diodes, Proceedings of the IEEE/Cornell Conference on Advanced Concepts in High Speed Semiconductor Devices and Circuits* (IEEE, Piscataway, NJ, 1989), p. 274–283.  
<sup>17</sup>P. G. Klemens, *Phys. Rev.* **148**, 845 (1966).  
<sup>18</sup>P. Roblin and M. W. Muller, *Phys. Rev. B* **32**, 5222 (1985).  
<sup>19</sup>W. Kohn and J. R. Onffroy, *Phys. Rev. B* **8**, 2485 (1973).  
<sup>20</sup>J. G. Gay and J. R. Smith, *Phys. Rev. B* **11**, 4906 (1975).  
<sup>21</sup>H. Kroemer and Qi-Gao Zhu, *J. Vacuum Sci. Technol.* **21**, 551 (1982).  
<sup>22</sup>P. Roblin, *Superlatt. Microstruct.* **4**, 363 (1988).  
<sup>23</sup>H. Fröhlich, *Proc. R. Soc. London, Ser. A* **160**, 230 (1937).  
<sup>24</sup>P. J. Turley and S. W. Teitsworth, *Phys. Rev. B* **44**, 3199 (1991).  
<sup>25</sup>S. Teitsworth, P. Turley, C. R. Wallis, W. Li, and P. Bhattacharya (unpublished).  
<sup>26</sup>C. Kittel, *Quantum Theory of Solids* (Wiley, New York, 1963).  
<sup>27</sup>Yu K. Pozhela and A. Reklaitis, *Solid-State Electron.* **23**, 927 (1980).  
<sup>28</sup>E. M. Conwell, in *Solid State Physics: Advances in Research and Applications*, edited by F. Seitz, D. Turnbull, and H. Ehrenreich (Academic, New York, 1967), Suppl. 9.  
<sup>29</sup>H. Sakaki, T. Noda, K. Hirakawa, M. Tanaka, and T. Matsusue, *Appl. Phys. Lett.* **51**, 1934 (1987).  
<sup>30</sup>P. E. Prange and T.-W. Lee, *Phys. Rev.* **168**, 779 (1968).  
<sup>31</sup>G. Bastard, *Wave Mechanics Applied to Semiconductor Heterostructures* (Les editions de Physique, Les Ulis, France, 1988).  
<sup>32</sup>L. Henrickson, K. Hirakawa, J. Frey, and T. Ikoma (unpublished).